Bioorganic & Medicinal Chemistry 18 (2010) 8485–8492

Contents lists available at ScienceDirect

Bioorganic & Medicinal Chemistry

journal homepage: www.elsevier.com/locate/bmc

# Thermodynamic and NMR analysis of inhibitor binding to dihydrofolate reductase

Ihor Batruch [a], Eliott Javasky [a], Eric D. Brown [b], Michael G. Organ [a], Philip E. Johnson [a,*]

[a] Department of Chemistry, York University, 4700 Keele St., Toronto, Ontario, Canada M3J 1P3
[b] Department of Biochemistry and Biomedical Sciences, McMaster University, 1200 Main St. West, Hamilton, Ontario, Canada L8N 3Z5

ARTICLE INFO

*Article history:*
Received 24 August 2010
Revised 13 October 2010
Accepted 18 October 2010
Available online 26 October 2010

*Keywords:*
DHFR inhibitor
Isothermal titration calorimetry
NMR spectroscopy
Binding thermodynamics

ABSTRACT

Isothermal titration calorimetry (ITC) was used to determine the thermodynamic driving force for inhibitor binding to the enzyme dihydrofolate reductase (DHFR) from *Escherichia coli*. 1,4-Bis-{[*N*-(1-imino-1-guanidino-methyl)]sulfanylmethyl}-3,6-dimethyl-benzene (**1**) binds DHFR:NADPH with a $K_d$ of 13 ± 5 nM while the related inhibitor 1-{[*N*-(1-imino-guanidino-methyl)]sulfanylmethyl}-3-trifluoromethyl-benzene (**2**) binds DHFR:NADPH with a $K_d$ of 3.2 ± 2.2 μM. The binding of these inhibitors has both a favorable entropy and enthalpy of binding. Additionally, we observe positive binding cooperativity between both **1** and **2** and the cofactor NADPH. Binding of compound **1** to DHFR is 285-fold tighter in the presence of the NADPH cofactor than in its absence. We did not detect binding of **2** to DHFR in the absence of NADPH. The backbone amide $^{1}H$ and $^{15}N$ NMR resonances of DHFR:NADPH and both DHFR:NADPH inhibitor complexes were assigned in order to better understand the binding of these inhibitors in solution. The chemical shift perturbations observed with the binding of **1** were greatest at residues closest to the binding site, but significant perturbations also occur away from the inhibitor location at amino acids in the vicinity of residue 58 and in the GH loop. The pattern of chemical shift changes observed with the binding of **2** is similar to that seen with **1**. The main differences in chemical shift perturbation between the two inhibitors are in the Met20 loop and in residues at the interface between the inhibitor and NADPH.



## 1. Introduction

Obtaining new inhibitors for medicinally important enzymes is an important goal in biological chemistry. The development of an effective inhibitor benefits from combining information from a multitude of sources such as structure–activity relationship (SAR) studies, high-resolution crystal structures of inhibitor–enzyme complexes, protein dynamics and knowing the thermodynamics of inhibitor binding. Determining the thermodynamics of inhibitor binding is most easily and accurately obtained from isothermal titration calorimetry (ITC) experiments.[1] Such data are important as it provides information about the driving forces involved in binding which, in turn, provides insight about the binding mechanism of the inhibitor. Additionally, the balance between the entropy and enthalpy of inhibitor binding is an important factor in drug development, with compounds of optimal potency having favorable enthalpy as well as entropy.[2,3]

DHFR is one of the most thoroughly studied enzymes to date.[4] It is responsible for maintaining intracellular 5,6,7,8-tetrahydrofolate (THF) at levels required for the biosynthesis of purines, pyrimidines and amino acids. Specifically, DHFR catalyzes the reduction of 7,8-dihydrofolate (DHF) to THF via hydride transfer from the nicotinamide adenine dinucleotide phosphate, reduced form (NADPH) cofactor to the C6 position of the pterin ring.[4] Since DHFR is essential for cell multiplication and growth, it has become a key target for anticancer, antibacterial, and antimalarial treatment, yielding drugs such as methotrexate, trimethoprim and pyrimethamine, respectively.[5]

DHFR is a small enzyme consisting of 159 amino acids with a tertiary structure consisting of four α-helices and one eight stranded β-sheet. The protein can be divided into two subdomains, the NADPH-binding domain (residues 38–88) and the major subdomain. The active site is located in the major subdomain and is responsible for ligand binding through interactions between the Met20 loop (residues 9–24), the F–G loop (residues 116–132) and the G–H loop (residues 142–150). The Met20 loop maintains the active site through hydrogen bonding with the two other loops and crystal structure analysis shows that this loop attains occluded, closed, open and disordered conformations. The occluded and closed forms

*Abbreviations:* DHF, 7,8-dihydrofolate; DHFR, dihydrofolate reductase; HSQC, heteronuclear single-quantum correlation; ITC, isothermal titration calorimetry; $K_d$, dissociation constant; NMR, nuclear magnetic resonance; $NADP^+$, nicotinamide adenine dinucleotide phosphate; NADPH, nicotinamide adenine dinucleotide phosphate, reduced form; sd, standard deviation; THF, 5,6,7,8-tetrahydrofolate.

* Corresponding author. Tel.: +1 416 736 2100x33119; fax: +1 416 736 5936.
*E-mail address:* pjohnson@yorku.ca (P.E. Johnson).

0968-0896/$ - see front matter © 2010 Elsevier Ltd. All rights reserved.
doi:10.1016/j.bmc.2010.10.048

are the dominant conformations. The closed conformation is evident in the DHFR:NADPH:DHF and DHFR:NADPH complexes while the occluded conformation is established by the DHFR:$NADP^+$:THF, DHFR:THF, and DHFR:NADPH:THF complexes.[6,7] Differences between these conformations is not just structural, but is also reflected in these states displaying different dynamic properties which, in turn, influences catalysis.[8–10]

Recently, two new competitive inhibitors, compound **1** and the related compound **2** (Fig. 1) have been identified by high throughput screening methods.[11] These molecules represent a new structural class of DHFR inhibitors as they are not based on a diaminoheterocycle chemical scaffold common to previously known DHFR inhibitors. Instead, these molecules have one or two isothiourea groups attached to a paradimethylbenzene core. Both compounds are competitive inhibitors of DHFR by binding at the active site in place of the DHF substrate.[11] The structures of both **1** and **2** bound to the DHFR:NADPH complex has been determined by X-ray methods and compound **1** was shown to interact with the Met20 loop, a mode of binding not seen with other DHFR inhibitors.[12] Interaction with the Met20 loop is particularly interesting as this loop plays an important role in the structural transitions that take place in the DHFR binding mechanism.[6,7] Here, we characterize the binding thermodynamics of the interaction of both compounds **1** and **2** with DHFR using ITC methods in order to understand the driving forces behind the interaction of these inhibitors with DHFR. Furthermore, in order to gain insight about interactions of inhibitors **1** and **2** with DHFR in solution, we have also assigned the backbone amide NMR chemical shifts of DHFR:NADPH inhibitor complexes.

## 2. Materials and methods

### 2.1. Protein expression and purification

The plasmid pFW117.1 containing the *folA* gene that encodes *Escherichia coli* DHFR was expressed in *E. coli* BL21 (DE3) Rosetta cells (Novagen). Unlabeled protein was produced in TYP media.[13] Biosynthetically $^{15}N$-labeled samples were prepared using M9 media containing 1 g/L of 99% $^{15}NH_4Cl$ (Cambridge Isotopes) and 1 g/L $^{15}N$ labeled Isogro algal extract (Isotec). $^{13}C/^{15}N$-labeled samples were prepared using M9 media containing 3.5 g/L [$^{13}C_6$] glucose (Cambridge Isotopes), 1 g/L of 99% $^{15}NH_4Cl$ and 1 g/L $^{13}C/^{15}N$ labeled Isogro. The 1 L bacterial cultures were grown in 1.8 L Fernbach flasks at 37 °C to an $OD_{600}$ of 0.6–0.7, induced with 1.0 mM IPTG, and incubated with shaking for 4 h.

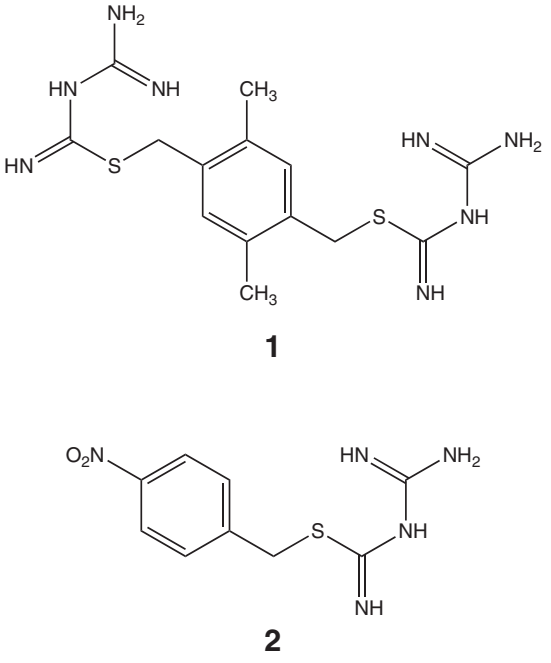


**Figure 1.** Chemical structures of the inhibitors **1** and **2** used in this study.

After induction, the cells were centrifuged and resuspended in lysis buffer (30 mM TRIS (pH 8), 1 M NaCl, 25% glycerol (v/v)) and the cells were lysed using a French pressure cell. Following centrifugation, the soluble fraction was filtered (0.45 μM) and dialysed against buffer A (20 mM TRIS (pH 6.2), 0.5 mM EDTA, 0.5 mM DTT) loaded onto a Q column (GE Healthcare) and eluted with a NaCl gradient of 0.1–1.0 M in buffer A. DHFR eluted at a concentration of 0.4 M NaCl. Fractions containing DHFR were then pooled and concentrated to 45 mL. $(NH_4)_2SO_4$ was added to a final concentration of 1 M. The DHFR solution was loaded atop a hydrophobic interaction column (GE Healthcare) that was previously equilibrated with a buffer containing 50 mM sodium phosphate (pH 7) and 1.0 M $(NH_4)_2SO_4$. DHFR was eluted during a 1.0–0.0 M $(NH_4)_2SO_4$ gradient with the DHFR displaced at 0.5 M $(NH_4)_2SO_4$. DHFR containing fractions were combined and concentrated to 1.8 mL and loaded onto a Sephacryl S-100 size-exclusion column (GE Healthcare). Pure DHFR was eluted with 100 mM sodium phosphate (pH 7) 150 mM NaCl, 5 mM $MgCl_2$, 0.5 mM EDTA, 0.02% (w/v) $NaN_3$. Finally, DHFR was concentrated and exchanged into NMR buffer (50 mM potassium phosphate (pH 6.8), 100 mM KCl, 1 mM EDTA, 4 mM DTT, 10% $^2H_2O$). Protein concentrations were determined using an $\varepsilon_{280}$ of 33810 $M^{-1}$ $cm^{-1}$.[14–16] The yields of unlabeled and isotopically labeled DHFR were approximately 10 and 6–10 mg/L of bacterial culture, respectively. Compounds **1** and **2** were obtained from Maybridge (Trevillett, UK).

### 2.2. NMR spectroscopy

DHFR samples for NMR spectroscopic analysis were exchanged into NMR buffer. Prior to use, this buffer was degassed and purged with argon. DTT was added to the NMR buffer after purging. NMR data was acquired on a 600 MHz Bruker Avance spectrometer using a $^1H$–$^{13}C$–$^{15}N$ triple resonance probe equipped with triple axis magnetic field gradients. All spectra were acquired at 25 °C, processed using NMRPipe[17] and analyzed with NMRView.[18]

The titration of NADPH (Sigma) into DHFR and titrations of compounds **1** or **2** into the DHFR:NADPH complex were monitored by recording a $^1H$, $^{15}N$ HSQC spectrum at each titration point. To help prevent air oxidation of the NADPH, the NADPH and inhibitor solutions were made using the degassed and argon-purged NMR buffer and the NMR sample was kept in an argon atmosphere. Additionally, solutions containing NADPH were shielded from light. If the $^1H$, $^{15}N$ HSQC spectrum showed that NADPH became oxidized during the course of the NMR experiments, additional NADPH was added. Molar ratios of DHFR to NADPH were typically 1:6–1:30. The molar ratio of DHFR to **1** varied between 1:1.3 and 1:1.7, and the final molar ratio of DHFR to **2** was 1:1. Chemical shift differences between resonances in the free and **1** and **2** inhibited forms were quantified using Eq. 1 where $\delta_{Hf}$ and $\delta_{Hb}$ are the frequency values of the $^1H$ resonances in the free and bound forms, respectively, and $\delta_{Nf}$ and $\delta_{Nb}$ are the frequency values of the $^{15}N$ resonances in the free and bound forms, respectively.[19]

$$\Delta\delta = \sqrt{(\delta_{Hf} - \delta_{Hb})^2 + \frac{(\delta_{Nf} - \delta_{Nb})}{6.5}} \quad (1)$$

Sequential assignments of the backbone amide and side-chain Cα/Cβ resonances for the binary DHFR:NADPH and ternary DHFR:NADPH:**1** complexes were made using $^{13}C/^{15}N$-labeled samples and using a combination of HNCACB,[20] CBCACONH[21] and HNCA[22] triple

resonance experiments. For all NMR experiments, the $^{1}H$ carrier was set to 4.7 ppm and the $^{15}N$ carrier to 118 ppm. For the CBCACONH and HNCAB experiments the $^{13}C$ carrier was set to 39 ppm, for the HNCA experiment the $^{13}C$ carrier was set to 54 ppm. In all NMR experiments, the $^{1}H$ spectral width used was 8928.6 Hz while the $^{15}N$ spectral width used was 2000.0 Hz. For the HNCAB and CBCACONH experiments, the $^{13}C$ spectral width used was 11312.2 Hz, while for the HNCA experiment the $^{13}C$ spectral width used was 4840.3 Hz. For the triple resonance experiments the total number of points in the $^{1}H$, $^{15}N$ and $^{13}C$ dimensions were 1280, 56 and 80, respectively.

### 2.3. Determination of binding constants by ITC

ITC experiments were performed using a MicroCal VP-ITC instrument. All samples were prepared in 50 mM potassium phosphate (pH 6.8), 100 mM KCl, 1 mM EDTA. The buffer used to dissolve NADPH, $NADP^{+}$, **1**, **2** was degassed using the MicroCal ThermoVac. Titrations were performed by injecting 36 consecutive 8 μL aliquots of ligand solution into the ITC cell containing DHFR. All ITC experiments were performed at 25 °C. For titrations of NADPH or $NADP^{+}$ into DHFR the concentration of cofactor used was 700–875 μM and 50–62 μM for DHFR. For titration of **1** into DHFR the concentrations used were 325 μM and 25 μM, respectively. For titrations of **1** into DHFR:NADPH the concentrations used were 140 μM and 10 μM, respectively. For titrations of **2** into DHFR:NADPH the concentrations used were 480 μM and 20 μM, respectively. For titrations of NADPH into DHFR:**1** or DHFR:**2** typical concentrations used were 280–300 μM and 10–22 μM, respectively. Enthalpy, equilibrium association constant and binding stoichiometry were determined by fitting the data, corrected for the heat of dilution of the titrant, to a 1:1 bimolecular interaction model using the program ORIGIN 5.0 (MicroCal Software Inc.).

## 3. Results

### 3.1. Thermodynamic analysis of inhibitor binding

The affinity and thermodynamic parameters of ligand and cofactor binding to DHFR were determined using ITC methods (Fig. 2). We also investigated the possibility of cooperative binding between ligand and cofactor by measuring the binding of both cofactor and ligand in the presence and absence of each other. The dissociation constant ($K_d$), $\Delta H$ and $\Delta S$ values for NADPH, $NADP^{+}$, **1** and **2** binding to apoenzyme as well as to different binary complexes are summarized in Table 1. The binding of the cofactors, NADPH and $NADP^{+}$, with apo-DHFR, the binary DHFR:**1** and DHFR:**2** complexes shows a negative enthalpy change ($\Delta H$) and a negative entropy change ($\Delta S$) indicating that the binding event is an exothermic process with entropic losses, hence it is enthalpically driven process. The dissociation constant ($K_d$) of cofactor NADPH to apo-DHFR is $(1.8 \pm 0.6) \times 10^{-6}$ M, while that of the oxidized cofactor, $NADP^{+}$, is $(1.3 \pm 0.1) \times 10^{-4}$ M. When NADPH was titrated into the DHFR:**1** and DHFR:**2** complexes, we still observed negative enthalpy and entropy, but the $K_d$ values were 7.5 and 6.0 times lower, respectively, than for NADPH binding to apo-DHFR, indicative of tighter binding. These results indicate that the presence of **1** or **2** enhances the affinity of DHFR for NADPH or $NADP^{+}$.

Inhibitor **1** binds tightly to the binary DHFR:NADPH complex, having a $K_d$ in the nanomolar range ($K_d = 13 \pm 5$ nM). Furthermore, a positive cooperativity with cofactor binding was observed as the DHFR:NADPH complex displayed a 285-fold tighter affinity for **1** than did apo-DHFR. Binding of **1** to the binary DHFR:$NADP^{+}$ complex ($K_d = 5.6 \pm 0.4$ μM) was much weaker than with DHFR bound to reduced cofactor but this binding still reflects weak positive

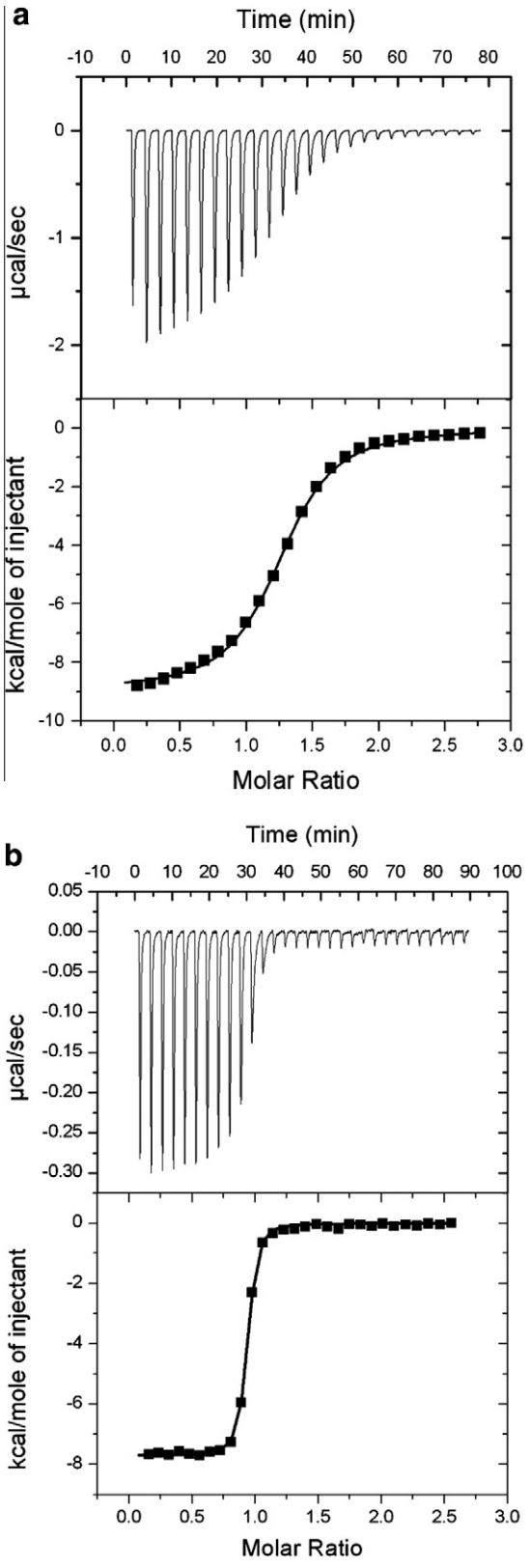


**Figure 2.** Analysis of ligand binding by DHFR using isothermal titration calorimetry. (a) Binding of NADPH to DHFR. (b) Binding of inhibitor **1** to a sample of the DHFR:NADPH complex. In both (a) and (b) shown on top is the raw titration data showing the heat resulting from each injection of NADPH or **1** into a DHFR or DHFR:NADPH solution. On the bottom are the integrated heats after correcting for the heat of dilution (squares). The line represents a non-linear least-squares fit to a 1:1 binding model.

**Table 1**
Dissociation constants and thermodynamic parameters of ligand binding for DHFR and DHFR complexes as determined by isothermal titration calorimetry[a]

| Sample | $K_d$ (M) | $\Delta H$ (cal mol$^{-1}$) | $\Delta S$ (cal mol$^{-1}$ deg$^{-1}$) |
|---|---|---|---|
| DHFR + NADPH | $(1.8 \pm 0.6) \times 10^{-6}$ | $(-1.1 \pm 0.3) \times 10^{4}$ | $-11 \pm 9$ |
| DHFR + NADP$^+$ | $(1.3 \pm 0.1) \times 10^{-4}$ | $(-2.3 \pm 1.4) \times 10^{4}$ | $-60 \pm 47$ |
| DHFR:NADPH + **1** | $(1.3 \pm 0.5) \times 10^{-8}$ | $(-7.2 \pm 2.2) \times 10^{3}$ | $12 \pm 7$ |
| DHFR:NADP$^+$ + **1** | $(5.6 \pm 0.4) \times 10^{-6}$ | $(-2.3 \pm 0.8) \times 10^{3}$ | $16 \pm 3$ |
| DHFR + **1** | $(3.7 \pm 2.4) \times 10^{-6}$ | $(-4.0 \pm 1.2) \times 10^{3}$ | $11 \pm 6$ |
| DHFR:**1** + NADPH | $(2.4 \pm 3.0) \times 10^{-7}$ | $(-1.08 \pm 0.05) \times 10^{4}$ | $-4 \pm 2$ |
| DHFR:NADPH + **2** | $(3.2 \pm 2.2) \times 10^{-6}$ | $(-2.0 \pm 0.2) \times 10^{3}$ | $19 \pm 2$ |
| DHFR + **2** | nbd | nbd | nbd |
| DHFR:**2** + NADPH | $(3.0 \pm 0.3) \times 10^{-7}$ | $(-1.1 \pm 0.2) \times 10^{4}$ | $-8 \pm 6$ |

[a] Data obtained at 25 °C and 50 mM potassium phosphate (pH 6.8), 100 mM potassium chloride, 1 mM EDTA. The values reported are averages of 2–9 individual experiments. The error range reported is one standard deviation. nbd signifies no measurable binding detected.

cooperativity of inhibitor binding that is 1.5 times tighter than **1** binding to apo-DHFR. The binding of **1** to apo and cofactor bound DHFR is both enthalpically and entropically favorable (Table 1).

In order to gauge the importance for DHFR inhibition of both isothiourea arms of compound **1** the binding of inhibitor **2** to DHFR was also analyzed using ITC methods. Compound **2** is an analog of **1**, it possesses only one isothiourea arm (Fig. 1). No measurable binding of **2** to apo-DHFR was detected, but binding of **2** to the DHFR:NADPH complex revealed a $K_d$ value in the micromolar range ($K_d$ = 3.2 ± 2.2 μM), a 246-fold reduction in binding affinity relative to **1**. Clearly, both isothiourea arms must be present for high affinity binding to be retained. Despite the difference in affinity between the two inhibitors the thermodynamics of **2** binding DHFR:NADPH shows the same trends as **1**, with binding having both favorable enthalpic and entropic components. The enthalpic contribution of **2** binding the DHFR:NADPH complex is 3.5-fold lower than for **1**. However, the positive entropic contribution of binding is greater for **2** than was the case for **1** binding DHFR:NADPH (Table 1).

### 3.2. Chemical shift mapping of inhibitor binding

The binding of **1** to NADPH-bound DHFR was readily detected by the observation of numerous changes in the $^1$H, $^{15}$N HSQC spectrum of DHFR:NADPH upon the addition of **1** (Fig. 3a). In order to identify the inhibitor binding site and better understand how inhibitor **1** binds DHFR, the backbone amide chemical shifts were assigned for the DHFR:NADPH and DHFR:NADPH:**1** complexes using HNCACB, CBCACONH and HNCA experiments. For the DHFR:NADPH complex, complete backbone amide assignments were obtained for all non-proline amino acids, with the exception of the N-terminal residue. In the DHFR:NADPH:**1** complex we were not able to obtain assignments for residues Met20, Ala29, Phe31, Trp47, Ile50 and Thr113, in addition to the proline residues and N-terminal amino acid. We note that there are no unassigned peaks present in the $^1$H, $^{15}$N HSQC of the DHFR:NADPH:**1** complex, and that the non-observance of these residues is likely due to them being severely line-broadened, and thus undetectable in the ternary complex. Binding of NADPH to DHFR and binding of **1** to DHFR:NADPH are in the slow exchange limit on the NMR time scale.

After determining the backbone assignments for the binary DHFR:NADPH complex and ternary DHFR:NADPH:**1** complex we then quantified the magnitude of the chemical shift changes on a per residue basis. We will note that chemical shift changes can result from either direct interaction of the nucleus with the ligand or indirectly from conformational changes upon ligand binding. Additionally, chemical shifts are a very sensitive indicator of conformational change. Large changes in chemical shift can result from a small structural change. With these caveats in mind, it is possible to gain insight into what effect ligand binding has on DHFR and the location of the binding site for **1** in the DHFR:NADPH complex.

Figure 3b shows the average weighted chemical shift change of **1** binding, plotted as a function of residue. The average per-residue change in chemical shift is calculated to be 0.083 ppm with a standard deviation of 0.117 ppm. Residues with a chemical shift change of greater than one standard deviation are highlighted in the backbone worm view of DHFR:NADPH:**1** (Fig. 3c and d). It is apparent from Figure 3 that backbone amide chemical shifts throughout DHFR are affected by the binding of **1**. Additionally, the regions of DHFR with the largest changes in chemical shift, and the residues that line-broaden with compound **1** binding are mostly located at the dihydrofolate-binding pocket. These include regions around residues 6 and 7; 16–32; 58 and 59; and residues 94–100.

For inhibitor **2**, the pattern of the chemical shift perturbations is similar to what we observed with compound **1** (Fig. 4). Residues throughout the protein have their chemical shift affected by the binding of **2**, with residues 6, 7, 22, 28, 30, 37, 46, 51, 58, 94 and 95 changing their chemical shift most. The average per-residue chemical shift is very similar for both inhibitors with inhibitor **2** having an average chemical shift perturbation of 0.0884 ppm with a standard deviation of 0.121 ppm.

Insight into the different effect the two ligands have on the DHFR amide chemical shifts can be seen from a difference plot between the changes in chemical shift for the two inhibitors (Fig. 5). The area with the most regular pattern of differences is located in residues in and adjacent to the Met20 loop (residues 7, 14, 16 and 23) where there are larger chemical shift perturbations seen with **1** binding than observed for compound **2**. Other significant differences between the two ligands are seen at residues 43, 46, 51, 58, 70, 95, 138 and 139 (Fig. 5).

## 4. Discussion

### 4.1. Thermodynamic analysis of inhibitor binding

Our study shows that inhibitor **1** binds tightly to the binary DHFR:NADPH complex, having a $K_d$ in the nanomolar range ($K_d$ = 13 ± 5 nM). This $K_d$ value is consistent with the previously determined $K_i$ value for compound **1** of 11.5 nM.[12] As compound **1** is a competitive inhibitor, these $K_i$ and $K_d$ values can be directly compared. Furthermore, a positive cooperativity with cofactor binding was observed as the DHFR:NADPH complex displayed a 285-fold tighter affinity for **1** than did apo-DHFR (Table 1). Binding of **1** to the binary DHFR:NADP$^+$ complex ($K_d$ = 5.6 ± 0.4 μM) was much weaker than with DHFR bound to reduced cofactor but this still reflects weak positive cooperativity of inhibitor binding that is 1.5 times tighter than **1** binding to apo-DHFR. The thermodynamic parameters for the binding of **1** to apo and cofactor bound DHFR are both enthalpically and entropically favorable. A typical ligand binding may be expected to be entropically unfavorable as two molecules free in solution form a complex. The entropic

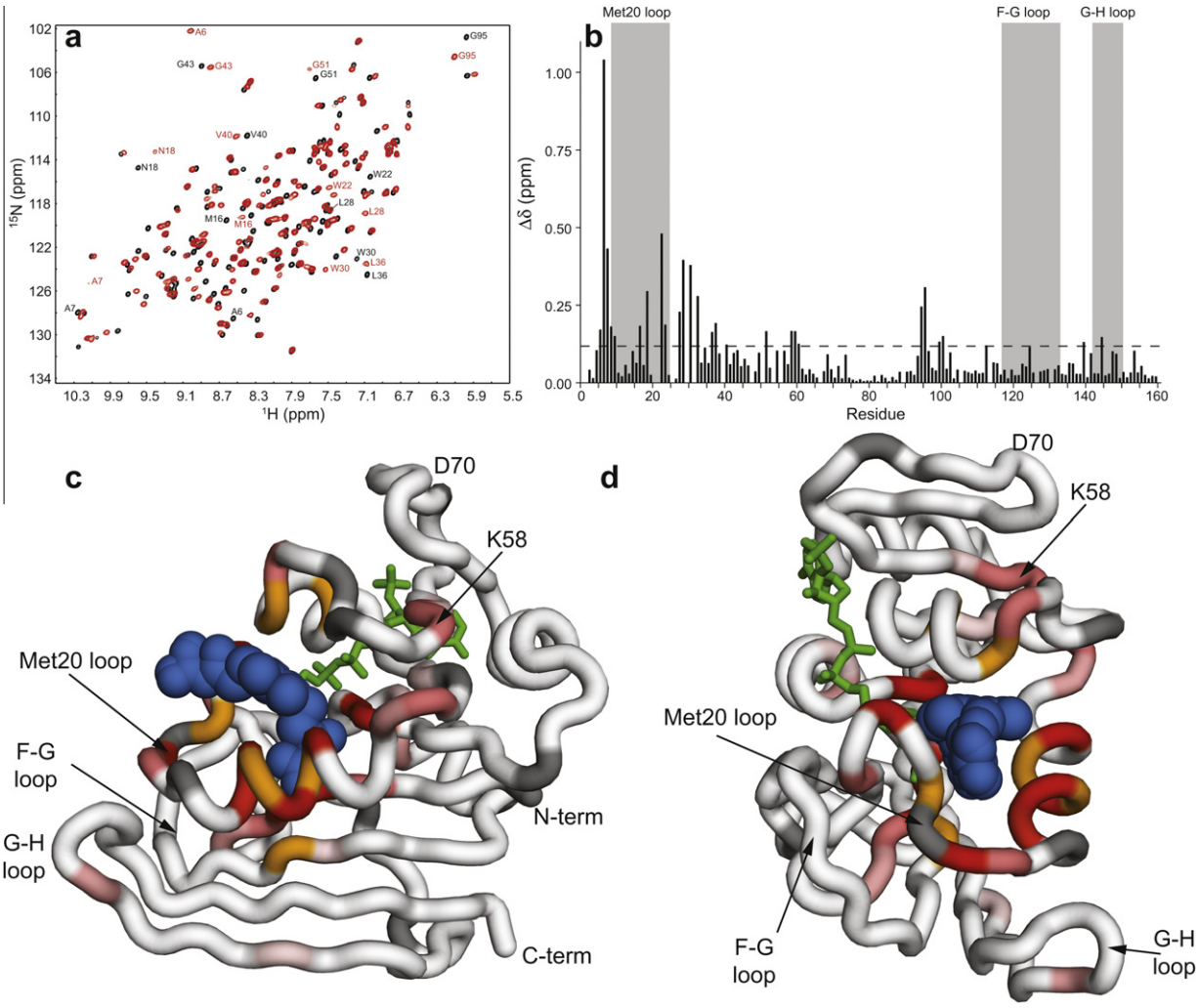


**Figure 3.** Chemical shift perturbations for the binding of **1** to DHFR. (a) Overlaid $^{1}H$, $^{15}N$ HSQC spectra of DHFR:NADPH (black) and DHFR:NADPH:**1** (red). Selected amides that show a large chemical shift change are labeled. (b) Histogram showing the difference in amide chemical shift changes with the binding of **1** to the DHFR:NADPH complex. The location of the Met20, F–G and G–H loops are indicated by shaded bars. The dashed line indicates the one sd level in $\Delta\delta$. (c and d) Structure of the DHFR:NADPH:**1** complex (pdb id: 2anq.pdb;[12]). NADPH is shown in green sticks while the inhibitor **1** is in blue sphere representation. Residues that experience a change in chemical shift greater than one sd with **1** binding are indicated in dark red with lighter shades of red indicating residues whose chemical shift are less affected by **1** binding. Residues in orange are those not detectable in the DHFR:NADPH:**1** complex due to line-broadening. Residues in white have changes in shift of 1 sd or less upon binding **1**. Residues in grey are proline.

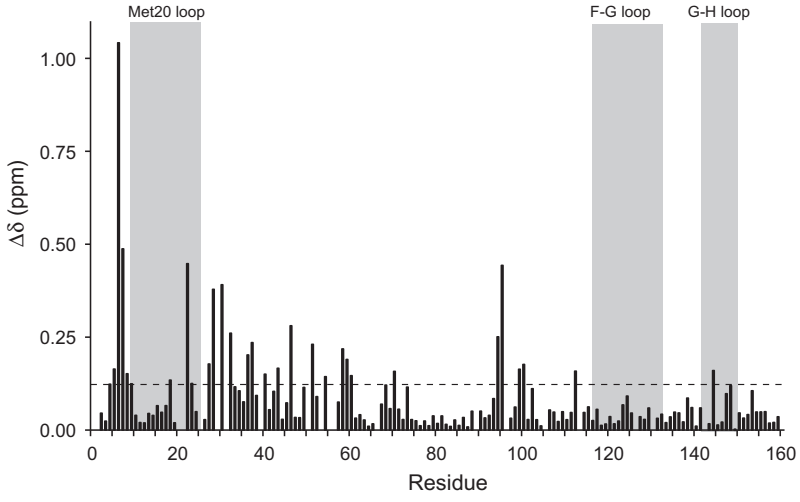


**Figure 4.** Histogram showing the normalized backbone amide chemical shift changes with the binding of compound **2** to the DHFR:NADPH complex. The location of the Met20, F–G and G–H loops are indicated by shaded bars. The dashed line indicates the one sd level in $\Delta\delta$.

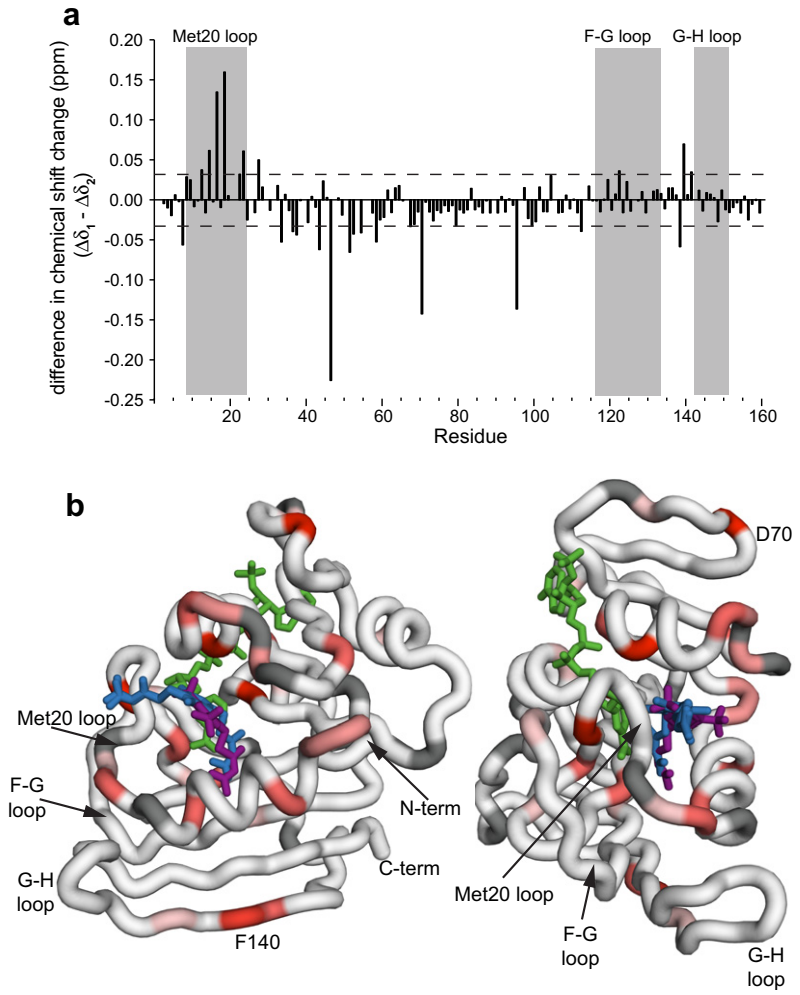


**Figure 5.** (a) Histogram showing the difference in the change in backbone amide chemical shift between **1** and **2**. The location of the Met20, F–G and G–H loops are indicated by shaded bars. The dashed line indicates the one sd level in the difference in $\Delta\delta$. (b) Structure of the DHFR:NADPH:**1** complex. NADPH is shown in green sticks while the inhibitor **1** is the blue stick. Superimposed is the structure of inhibitor **2** as purple sticks. Residues that experience the greatest difference in chemical shift change between **1** and **2** are indicated in dark red with lighter shades of red indicating residues whose chemical shift differences are lower. Residues in grey are proline.

contribution to binding of **1** to DHFR likely results from release of ordered water molecules from the hydrophobic portions of the binding pocket. In support of this possibility we calculated the total polar and apolar surface area in the free compound **1**, the binary DHFR:NADPH complex and ternary DHFR:NADPH:**1** complex. The total amount of apolar surface area dropped 402 Å$^2$ going from the free compound **1** and binary complex state to the ternary complex.

The binding of inhibitor **2** to DHFR was also analyzed with ITC methods. Compound **2** is an analog of **1**, it possesses only one isothiourea arm (Fig. 1).[12] No measurable binding of **2** to apo-DHFR was detected, but binding of **2** to the DHFR:NADPH complex revealed a $K_d$ value in the micromolar range ($K_d = 3.2 \pm 2.2$ μM), a 246-fold reduction in binding affinity relative to **1**. The two isothiourea arms must be present in the inhibitor for high affinity binding to be retained. Despite the difference in affinity between the two inhibitors, the thermodynamics of **2** binding DHFR:NADPH shows the same trends as **1**. Binding of **2** has both favorable enthalpic and entropic components (Table 1). The enthalpic contribution of **2** binding the DHFR:NADPH complex is 3.5-fold lower than for **1**, likely reflecting the presence of fewer ionic and hydrogen bonds forming with **2** than **1**. However, the positive entropic contribution of binding is greater for **2** than was the case for **1** binding DHFR:NADPH.

The affinity of DHFR:NADPH for **1** is on par with known inhibitors of DHFR such as methotrexate, whose $K_d$ ranges from $10^{-8}$ M to less than $10^{-11}$ M depending on the presence of cofactors and the source of DHFR,[23–25] trimethoprim (( *Lactobacillus casei* DHFR) $5 \times 10^{-8}$ M)[24] and trimetrexate ((*L. casei* DHFR) $\sim 5 \times 10^{-9}$ M).[26] The binding data for both **1** and **2** indicates that presence of the cofactor, NADPH, leads to large positive binding cooperativity. This positive cooperativity seems to be a general feature for competitive inhibitors of DHFR, it was also seen with methotrexate,[24,27] and likely results from the direct interaction of the inhibitor and cofactor when bound. In the structure of the complex between DHFR and both inhibitors, the nicotinamide ring of NADPH stacks perpendicularly with the ring structure of the inhibitor.[12] Mechanistically, having the cofactor in close contact with the DHF substrate facilitates catalysis. This contact with NADPH is similarly exploited by the binding mechanism of many high affinity DHFR inhibitors.

The binding of the cofactors, NADPH and NADP$^+$, with both apo-DHFR, and the binary DHFR:**1** and DHFR:**2** complexes revealed a negative enthalpy change ($\Delta H$) and a negative entropy change ($\Delta S$) indicating that the binding event is an exothermic process with entropic losses, hence binding is enthalpically driven (Table 1). The dissociation constant ($K_d$) of cofactor NADPH to apo-DHFR is $(1.8 \pm 0.6) \times 10^{-6}$ M, while that of the oxidized cofactor, NADP$^+$, is $(1.3 \pm 0.1) \times 10^{-4}$ M. The 72-fold weaker binding of NADP$^+$ to

apo-DHFR than that of NADPH, is exactly the same ratio as reported by Fierke et al.[23] A possible cause for weaker binding of $NADP^+$ compared to NADPH is the positive charge on the nicotinamide ring of $NADP^+$ that interferes with binding in the hydrophobic cofactor binding pocket.[28]

When NADPH was titrated into the DHFR:**1** and DHFR:**2** complexes, we still observed negative enthalpy and entropy values of binding, but the $K_d$ values were 7.5 and 6.0 times lower, respectively, than for NADPH binding to apo-DHFR, indicative of tighter binding (Table 1). These results indicate that the presence of the inhibitors **1** and **2** enhances the affinity of DHFR for NADPH. Again, this likely results from interactions between the cofactor and inhibitor when both are bound, as observed in the crystal structure.[12] A positive cooperativity between the inhibitor methotrexate and the cofactor was also seen by Birdsall et al. for *L. casei* DHFR.[24]

### 4.2. Chemical shift mapping of inhibitor binding

The chemical shift perturbations observed with the binding of compound **1** can be arranged into two groups. In the first are the residues closest to the inhibitor. Inhibitor binding directly influences these amino acids. The second group consists of residues located away from the ligand-binding site. These amino acids are indirectly influenced by the inhibitor and may reflect subtle changes in structure or changes in the dynamics of the protein.

As shown in Figure 3, the regions of the DHFR:NADPH complex that experience the largest chemical shift changes are residues 6 and 7, residues between amino acids 16–32, residues 58 and 59; and residues 94–100. When compared with the crystal structure of the ternary DHFR:NADPH:**1** complex[12] most of the residues that experience the largest chemical shift changes are clustered in close proximity to the inhibitor (Fig. 3c and d). Analysis of the X-ray structure of the DHFR:NDPH:**1** complex (2anq.pdb) shows that one isothiourea group of **1** interacts with a region that would form the binding pocket of the pteridine ring of a substrate molecule, interacting with residues 5, 7, 20, 27, 31, 94, 100 and 113. The other isothiourea group interacts with a region in DHFR unknown to interact with folate analogues or other inhibitors of DHFR. This flexible second isothiourea group protrudes out of the binding cavity to make contacts with the Met20 loop, making van der Waals contacts with residues 19, 20, 28, 49 and 50. Compound **1** also interacts with the cofactor NADPH.[12] These residues that interact with **1** are all among the residues that experience the largest chemical shift changes with ligand binding. This indicates that the binding site for **1** in solution by NMR spectroscopy closely matches the X-ray structure.

As shown in Figure 3, the residues whose line widths increase to such an extent that the they are not visible in the inhibitor **1**–DHFR complex (20, 29, 31, 47, 50 and 113) are adjacent to the bound inhibitor and, with the exception of residue 20, not found in the loop regions that regulate entry into the active site. A recent study of the dynamics of DHFR in the presence of the inhibitors methotrexate and trimethoprim showed that some of these same or adjacent residues (29, 31, 112) showed significant $R_2$ dispersion values in the inhibited form.[29] This implies our inhibitor 1 may have a similar affects on the dynamics of DHFR at these locations as seen for methotrexate. Future NMR based relaxation studies will explore this possibility.

In the group of residues that experience the largest chemical shift changes are residues 16, 58 and 59. These residues do not make direct contact with the inhibitor. Residue 16 does not contact **1** in the crystal structure but packs against the Met20 loop, which does contact the inhibitor. It is likely that the chemical shift changes experienced by residue 16 are influenced by **1** binding via its interactions with the Met20 loop. Residues 58 and 59 are far from the inhibitor binding site and the side-chains of these residues do not make contact with **1**. The perturbation for these shifts may result from mobility of inhibitor in the binding site or from minor structural changes triggered by inhibitor binding. However, the lack of residues neighboring 58 and 59 also experiencing significant chemical shift changes argues against this. An alternate possibility is that the protein dynamics at residues 58 and 59 may be affected by **1** binding and this is reflected in the chemical shifts. Although not involved in binding of **1**, this region is important for substrate binding with large chemical shift changes seen upon folate binding to DHFR.[30] Additional support for the significance of the region near residue 58 being affected by inhibitor binding is due to its cross-strand proximity to M42. This residue, though removed from direct contact with substrate or inhibitor, has been proposed as a key hub for DHFR dynamics.[31] It is possible that inhibitor binding effects are sensed by M42, are then transmitted to residue 58, and then are manifested as chemical shift perturbations. These sorts of questions and the role in dynamics played by compounds **1** and **2** will be addressed by future NMR relaxation studies of DHFR with and with inhibitor.

The data presented here also allows a comparison of the chemical shift perturbation effects in DHFR:NADPH due to binding by two analogous inhibitors, compounds **1** and **2**. Significant differences between the chemical shift perturbations with **1** and **2** binding are at the interface between the inhibitor, and NADPH and adjacent to the inhibitor binding site. These differences likely arise due to subtle differences between the binding modes of the two compounds. Additional significant differences are around residue 140. These changes likely arise through the side-chain interaction of W30, a residue that is in the helix adjacent to the active site and residue F140.

In the crystal structures of the two complexes, compound **1** makes contact with the Met20 loop, but **2** does not.[12] This binding difference is reflected in the chemical shift perturbations for compound **2** (Fig. 4). There is a greater effect of **1** binding in the Met20 loop than that seen with the binding of **2** (Fig. 5). What is noteworthy is that residues in the Met20 loop still experience chemical shift changes in the Met20 loop with **2** binding (Fig. 4) despite this contact not being seen in the crystal structure. This chemical shift change in the Met20 loop could reflect mobility of the inhibitor in the active site, or changes in the dynamics of the protein with the binding of **2** being reflected in the chemical shifts in the Met 20 loop.

## 5. Conclusions

In conclusion, we have analyzed the binding thermodynamics of two chemically related inhibitors of DHFR that possess a chemical structure distinct from other DHFR inhibitors. Binding of these molecules is both an entropically and enthalpically favorable process and shows cooperative binding with the NADPH cofactor. NMR chemical shift perturbations with ligand binding are greatest in the immediate vicinity of the bound inhibitor. However, significant perturbations are also observed for residues located away from the inhibitor such as near K58 and in the GH loop. Given the important role played by protein dynamics during DHFR catalysis, future studies will investigate how inhibitor binding affects these motions.

## Acknowledgements

We thank Murray Junop (McMaster University) for useful discussions, Miguel Neves for help in preparing Figure 2 and Tony Tavares for critical reading of this manuscript. This work was supported by funding from the Natural Sciences and Engineering

Research Council of Canada (NSERC) to P.E.J., and the Ontario Research and Development Challenge Fund (ORDCF) to M.G.O.

## References and notes


1. Chaires, J. B. *Annu. Rev. Biophys.* **2008**, *37*, 135.
2. Freire, E. *Drug Discovery Today* **2008**, *13*, 869.
3. Ruben, A. J.; Kiso, Y.; Freire, E. *Chem. Biol. Drug Des.* **2006**, *67*, 2.
4. Schnell, J. R.; Dyson, H. J.; Wright, P. E. *Annu. Rev. Biophys. Biomol. Struct.* **2004**, *33*, 119.
5. Feeney, J. *Angew. Chem., Int. Ed.* **2000**, *39*, 290.
6. Sawaya, M. R.; Kraut, J. *Biochemistry* **1997**, *36*, 586.
7. Venkitakrishnan, R. P.; Zaborowski, E.; McElheny, D.; Benkovic, S. J.; Dyson, H. J.; Wright, P. E. *Biochemistry* **2004**, *43*, 16046.
8. McElheny, D.; Schnell, J. R.; Lansing, J. C.; Dyson, H. J.; Wright, P. E. *Proc. Natl. Acad. Sci. U.S.A.* **2005**, *102*, 5032.
9. Boehr, D. D.; McElheny, D.; Dyson, H. J.; Wright, P. E. *Science* **2006**, *313*, 1638.
10. Boehr, D. D.; McElheny, D.; Dyson, H. J.; Wright, P. E. *Proc. Natl. Acad. Sci. U.S.A.* **2010**, *107*, 1373.
11. Zolli-Juran, M.; Cechetto, J. D.; Hartlen, R.; Daigle, D. M.; Brown, E. D. *Bioorg. Med. Chem. Lett.* **2003**, *13*, 2493.
12. Summerfield, R. L.; Daigle, D. M.; Mayer, S.; Mallik, D.; Hughes, D. W.; Jackson, S. G.; Sulek, M.; Organ, M. G.; Brown, E. D.; Junop, M. S. *J. Med. Chem.* **2006**, *49*, 6977.
13. Sambrook, J.; Fritsch, E. F.; Maniatis, T. *Molecular Cloning: A Laboratory Manual*; Cold Spring Harbor, N.Y.: Cold Spring Harbor Laboratory Press, 1989.
14. Edelhoch, H. *Biochemistry* **1967**, *6*, 1948.
15. Gill, S.; vonHippel, P. *Anal. Biochem.* **1989**, *182*, 319.
16. Pace, C. N.; Vajdos, F.; Fee, L.; Grimsley, G.; Gray, T. *Protein Sci.* **1995**, *4*, 2411.
17. Delaglio, F.; Grzesiek, S.; Vuister, G. W.; Zhu, G.; Pfeifer, J.; Bax, A. *J. Biomol. NMR* **1995**, *6*, 277.
18. Johnson, B. A.; Blevins, R. A. *J. Biomol. NMR* **1994**, *4*, 603.
19. Mulder, F. A. A.; Schipper, D.; Bott, R.; Boelens, R. *J. Mol. Biol.* **1999**, *292*, 111.
20. Wittekind, M.; Mueller, L. *J. Magn. Reson., Ser. B* **1993**, *101*, 201.
21. Grzesiek, S.; Bax, A. *J. Am. Chem. Soc.* **1992**, *114*, 6291.
22. Grzesiek, S.; Bax, A. *J. Magn. Reson.* **1992**, *96*, 432.
23. Fierke, C. A.; Johnson, K. A.; Benkovic, S. J. *Biochemistry* **1987**, *26*, 4085.
24. Birdsall, B.; Burgen, A. S. V.; Roberts, G. C. K. *Biochemistry* **1980**, *19*, 3723.
25. Schweitzer, B. I.; Dicker, A. P.; Bertino, J. R. *FASEB J.* **1990**, *4*, 2441.
26. Polshakov, V. I.; Birdsall, B.; Frenkiel, T. A.; Gargaro, A. R.; Feeney, J. *Protein Sci.* **1999**, *8*, 467.
27. Bystroff, C.; Kraut, J. *Biochemistry* **1991**, *30*, 2227.
28. Matthews, D. A.; Alden, R. A.; Freer, S. T.; Xuong, N.; Kraut, J. *J. Biol. Chem.* **1979**, *254*, 4144.
29. Mauldin, R. V.; Carroll, M. J.; Lee, A. L. *Structure* **2009**, *17*, 386.
30. Osborne, M. J.; Venkitakrishnan, R. P.; Dyson, H. J.; Wright, P. E. *Protein Sci.* **2003**, *12*, 2230.
31. Mauldin, R. V.; Lee, A. L. *Biochemistry* **2010**, *49*, 1606.